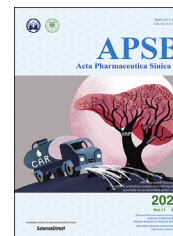




Chinese Pharmaceutical Association
Institute of Materia Medica, Chinese Academy of Medical Sciences

Acta Pharmaceutica Sinica B

www.elsevier.com/locate/apsb
www.sciencedirect.com



ORIGINAL ARTICLE

An injectable micelle-hydrogel hybrid for localized and prolonged drug delivery in the management of renal fibrosis



Xianyan Qin^{a,b,†}, Yingying Xu^{a,†}, Xu Zhou^{a,c}, Tao Gong^a,
Zhi-Rong Zhang^a, Yao Fu^{a,*}

^aKey Laboratory of Drug-Targeting and Drug Delivery System of the Education Ministry and Sichuan Province, Sichuan Engineering Laboratory for Plant-Sourced Drug and Sichuan Research Center for Drug Precision Industrial Technology, West China School of Pharmacy, Sichuan University, Chengdu 610041, China

^bKey Laboratory of Advanced Technologies of Materials, Ministry of Education and School of Materials Science and Engineering, Southwest Jiaotong University, Chengdu 610031, China

^cSichuan Provincial Orthopedic Hospital, Chengdu 610041, China

Received 23 June 2020; received in revised form 4 September 2020; accepted 28 September 2020

KEY WORDS

Hydrogel;
“Plum–pudding”
structure;
Localized therapy;
Controlled release;
Renal fibrosis;
Inflammation;
Celastrol;
Anti-TGF β antibody

Abstract Localized delivery, comparing to systemic drug administration, offers a unique alternative to enhance efficacy, lower dosage, and minimize systemic tissue toxicity by releasing therapeutics locally and specifically to the site of interests. Herein, a localized drug delivery platform (“plum–pudding” structure) with controlled release and long-acting features is developed through an injectable hydrogel (“pudding”) crosslinked *via* self-assembled triblock polymeric micelles (“plum”) to help reduce renal interstitial fibrosis. This strategy achieves controlled and prolonged release of model therapeutics in the kidney for up to three weeks in mice. Following a single injection, local treatments containing either anti-inflammatory small molecule celastrol or anti-TGF β antibody effectively minimize inflammation while alleviating fibrosis *via* inhibiting NF- κ B signaling pathway or neutralizing TGF- β 1 locally.

Abbreviations: α -SMA, α -smooth muscle actin; bis-F127-MA, bis-F127-methacrylate; BSA, bovine serum albumin; CLT, celastrol; Cy5.5-NHS, cyanine 5.5-*N*-hydroxysuccinimide; DAPI, 4',6-diamidino-2-phenylindole; DEX, dexamethasone; DiD, 1,1'-dioctadecyl-3,3,3',3'-tetramethylindodicarbocyanineperchlorate; ECM, extracellular matrix; EDCl, carbodiimide hydrochloride; ESR, equilibrium swelling ratio; FITC, fluorescein isothiocyanate; G' , storage modulus; G'' , the loss modulus; HA, hyaluronic acid; HASH, thiolated hyaluronic acid; iNOS, nitric oxide synthase; IL-6, interleukin 6; IL-1 β , interleukin 1 β ; MOD, mean optical density; NHS, *N*-hydroxysuccinimide; RIF, renal interstitial fibrosis; PDI, polydispersity index; RSR, real-time swelling ratio; SEM, scanning electron microscopy; SD, standard deviation; TEM, transmission electron microscopy; TNF- α , tumor necrosis factor α ; TGF- β 1, transforming growth factor β 1; TUNEL, terminal deoxynucleotidyl transferase dUTP nick end labelling; UO, unilateral ureteral obstruction.

*Corresponding author.

E-mail address: yfu4@scu.edu.cn (Yao Fu).

[†]These authors made equal contributions to this work.

Peer review under responsibility of Institute of Materia Medica, Chinese Academy of Medical Sciences and Chinese Pharmaceutical Association.

<https://doi.org/10.1016/j.apsb.2020.10.016>

2211-3835 © 2021 Chinese Pharmaceutical Association and Institute of Materia Medica, Chinese Academy of Medical Sciences. Production and hosting by Elsevier B.V. This is an open access article under the CC BY-NC-ND license (<http://creativecommons.org/licenses/by-nc-nd/4.0/>).

Importantly, the micelle-hydrogel hybrid based localized therapy shows enhanced efficacy without local or systemic toxicity, which may represent a clinically relevant delivery platform in the management of renal interstitial fibrosis.

© 2021 Chinese Pharmaceutical Association and Institute of Materia Medica, Chinese Academy of Medical Sciences. Production and hosting by Elsevier B.V. This is an open access article under the CC BY-NC-ND license (<http://creativecommons.org/licenses/by-nc-nd/4.0/>).

1. Introduction

Systemic drug administration often faces premature release and nonspecific distributions resulting in lower efficacy and off-target toxicity. Localized delivery offers an alternative to enhance efficacy, lower dosage, and minimize systemic tissue toxicity by locally releasing therapeutics specifically to the site of interests. Langer and colleagues^{1–3} pioneered the technology of polymer-based drug delivery depots to directly deliver therapeutics to the disease site in a controlled manner. However, some require preformulation under harsh chemical conditions and complex surgical interventions to place the implants^{4,5}. As an alternative, injectable hydrogels are gaining attentions over a broad range of applications such as cellular scaffolds, controlled biomolecule delivery, soft tissue replacements, and wound dressings^{6,7}. Specifically, hydrogel precursors and therapeutics are injected in the solution form, which then undergo *in situ* gelation *via* either physical or chemical crosslinking. However, due to their loose structure and hydrophilic nature, localized hydrogel systems disfavor hydrophobic drugs and usually incorporate small molecules *via* covalent conjugation which relies on heavy chemistry resulting in undesired toxicity^{8,9}.

Inspired by advances in biomedical engineering and nanotechnology, we proposed an injectable micelle-hydrogel hybrid for noncovalently encapsulating hydrophobic drugs to achieve localized controlled drug release. In this system, terminal functionalized triblock polymeric micelles not only carry on hydrophobic small molecules, but function as hydrogel crosslinkers, displaying a novel “plum–pudding” structure (Scheme 1). Such a material system is characterized by randomly dispersed micellar nanoparticles (“plums”, content: 50%) in a conventional hydrogel network (“pudding”). With this type of design, poorly water-soluble molecules can be easily encapsulated in the hydrophobic micellar core *via* hydrophobic interaction. Together, the micelle-crosslinked hydrogel hybrid can serve as a reservoir for hydrophobic solutes to achieve controlled and prolonged release. Additionally, the hydrogel network maintains the nature of rationally modulated mesh sizes which provides proper control over the mass transport of biomolecules and the potential of cell therapy.

In recent years, anti-fibrosis drug research mainly focuses on the development of small molecules and antibodies macromolecules. At present, more than 30 small molecule drugs targeting different molecular targets are in the pre-clinical and clinical research stage, involving molecular targets including kinases, growth factors, chemokines, lipid regulation, proteases, ion channels, nuclear factor receptors, etc.^{10,11}. For highly specific kinase inhibitors, treatment concentrations need to be carefully selected to avoid or reduce adverse effects due to “off-target” distribution. There are also problems with inhibitors of single growth factors. For example, the tyrosine kinase inhibitor imatinib works by inhibiting the platelet growth factor (PDGF) pathway,

but its phase II clinical trials for idiopathic pulmonary fibrosis (IPF) and systemic sclerosis (SSc) have failed¹². Currently, the first-line treatment for renal interstitial fibrosis (RIF) mainly focuses on the renin-angiotensin-aldosterone system, including angiotensin-converting enzyme inhibitors, angiotensin II receptor 1 antagonists, and direct renin blockers, and it is limited to reducing symptoms and delaying the progression of RIF^{13–16}.

In the present study, we applied the unique hydrogel–micelle hybrid system to locally deliver therapeutics for the management of RIF in mice. Celastrol (CLT), a natural compound extracted from *Tripterygium wilfordii*, was selected as a model therapeutic for the treatment of RIF due to its excellent anti-inflammatory and antiproliferation activities^{17–19}. Our laboratory previously reported an albumin nanoparticle with a well-defined size achieving site-specific delivery of CLT to mesangial cells for the treatment of mesangioproliferative glomerulonephritis²⁰. Without a proper carrier system, CLT following intravenous administration often resulted in dose-related systemic toxicities possibly *via* interaction with multiple cellular targets^{21,22}. In this work, we developed a hyaluronic acid-derived hydrogel hybrid crosslinked by terminally functionalized Pluronic micelles to achieve localized and prolonged release of CLT in the kidney. In addition, due to the critical role of TGF- β during fibrosis²³, anti-TGF β antibody was selected as a model biomolecule to further demonstrate the sustained therapeutic effect of the localized delivery strategy against RIF using a unilateral ureteral obstruction (UO) mice model.

2. Materials and methods

2.1. Materials

Pluronic® F127 (molecular weight 12,600 Da) was purchased from BASF (Tarrytown, USA). Sodium hyaluronate (HA, molecular weight 77 kDa) was provided by Bloomage Biotechnology Corporation Limited (Ji’nan, China). *N*-Hydroxysuccinimide (NHS), *N*-(3-dimethylaminopropyl)-*N*’-ethylcarbodiimide hydrochloride (EDCI), and cysteamine hydrochloride (CHS·HCl) were obtained from Sigma–Aldrich (USA). Methacrylic anhydride (MA) was purchased from Best-Reagent (Chengdu, China). Bovine serum albumin (BSA) was provided by Biosharp (Hefei, China). Cyanine 5.5-*N*-hydroxysuccinimide (Cy5.5-NHS) was purchased from Hypercyte (Beijing, China). Celastrol (CLT) was obtained from Must Biotechnology (Chengdu, China), and murine monoclonal anti-TGF β 1 antibody was provided by R&D (Minneapolis, MN, USA).

2.2. Synthesis of hydrogel precursors

Bis-F127-methacrylate (bis-F127-MA) was synthesized according to Supporting Information Scheme S1. Briefly, F127 (5 g, 0.4 mmol) was dissolved in 100 mL of anhydrous dichloromethane in a round bottom dry flask followed by dropwise

addition of 2 mL of triethylamine and methacrylic anhydride (4 mL, 0.026 mol) under ice bath. After stirring for 24 h at room temperature, the reaction mixture was concentrated to 20 mL *via* rotary evaporation, precipitated in cold diethyl ether, and then dried in vacuum. The obtained bis-F127-MA (yield: 80.2%) was validated by ^1H NMR (400 MHz, CDCl_3 , δ): 6.13 (s, 2H), 5.58 (s, 2H), 3.57 (bs, PEG), 1.13 (bs, 6H) (Supporting Information Fig. S1).

Thiolated hyaluronic acid (HASH) was obtained following a pre-established method (Supporting Information Scheme S2)²⁴. The obtained product (yield: 89.9%) was validated by ^1H NMR (400 MHz, D_2O , δ): 4.38 (bs, 2H), 3.0–3.8 (bs, 5H), 2.54 (m, 2H), 2.30 (m, 2H), 1.87 (bs, 3H) (Supporting Information Fig. S2).

2.3. Gelation and characterizations of physicochemical properties

2.3.1. Preparation of hydrogel

F127 micelle crosslinked hydrogel (F127-HA) was synthesized *via* Michael addition between thiol residuals on the HA backbone and the terminal methacrylate on bis-F127-MA. Briefly, bis-F127-MA micelles were produced by a thin film-dispersion method. First, 100 mg of bis-F127-MA was dissolved in 10 mL of acetonitrile in a 50 mL round bottom flask, evaporated *via* rota-vap at 45 °C to form a thin film, then hydrated in 2 mL of HEPES to afford a micelle dispersion (pH 8.0), which was then mixed with HASH in ddH₂O of various concentrations, *e.g.*, 1%, 5%, and 10% (*w/v*). Pregel solutions were quickly mixed at equal volume and allowed to gel at 37 °C, and gelation was assessed by the standard vial tilting method²⁵.

To load therapeutic components, 8 mg of CLT and 100 mg of bis-F127-MA were dissolved in the organic solvent such as acetonitrile prior to thin film formation, which was then subjected to hydration in 2 mL of HEPES to afford CLT loaded 5% (*w/v*) bis-F127-MA micelles, while anti-TGF β 1 antibody was dissolved in 5% (*w/v*) HASH solutions. The final concentrations of CLT and anti-TGF β 1 antibody were 4 and 6.7 mg/mL, respectively. After two parts were fully mixed in equal volume, the gel precursor solution was then ready for injection in mice.

2.3.2. Characterization of rheological properties

The gelation kinetics was monitored by rheometric study. The following rheological measurements were carried out at 37 °C on a Haake Mars Modular Advanced Rheometer (Thermo Fisher Scientific, USA). A time sweep mode was adopted (frequency, 1 Hz; strain, 5%) to determine the sol–gel transition point, using a parallel plate setting (diameter, 40 mm; gap, 1000 μm). Next, at a fixed strain of 5%, a frequency sweep test was performed from 0.1 to 10 Hz to measure the storage modulus (G'), and loss modulus (G''). The frequency range was ensured to stay in the linear viscoelastic region of each hydrogel sample as determined by amplitude sweeps (data not shown). To determine the injectability of such hydrogel hybrids, the viscosity of hydrogel precursor solutions was determined using a standard viscometer (Brookfield, HBDV-II+PRO, USA) as previously described²⁶.

2.3.3. Characterization of hydrogel microstructure

The hydrogel samples were frozen in liquid nitrogen and then lyophilized. The cross-sections of lyophilized hydrogels were sputter-coated with gold, and subjected to observation under scanning electron microscopy (SEM, JSM-7500F, JEOL, Japan) as previously described²⁷.

2.3.4. *In vitro* swelling

To perform swelling studies, hydrogel discs were fabricated, freeze-dried and weighed (W_d). Next, 3 mL of 1 \times PBS (10 mmol/L, pH 7.4) was added to the lyophilized hydrogel to allow swelling at 37 °C. At each given time point, hydrogel disks were removed, the surface water was carefully blotted with filter paper, and the wet weight (W_t) of each hydrogel disk was recorded. The real-time swelling ratio (RSR) has been calculated according to the following Eq. (1):

$$\text{RSR}(\%) = \frac{W_t - W_d}{W_d} \times 100 \quad (1)$$

2.3.5. *In vitro* degradation

To explore hydrogel degradation profiles *in vitro*, fully cured F127-HA hydrogels were lyophilized, and the lyophilized samples were placed in 10 mL of 1 \times PBS (10 mmol/L, pH 7.4) to allow swelling and degradation at 37 °C. The weight of lyophilized hydrogel was recorded as W_0 , which was allowed to swell in the buffer solution over time. At each given time point, the hydrogel sample was collected, freeze-dried and the gel weight at time t was recorded as W_t . The degradation profile of F127–HA hydrogel hybrid was presented as the percentage of weight loss (W_{loss} , %) calculated by the following Eq. (2):

$$W_{\text{loss}}(\%) = \frac{W_t - W_0}{W_0} \times 100 \quad (2)$$

2.4. *In vitro* release

As mentioned in Section 2.3, 1 mg of DiD and 100 mg of bis-F127-MA were dissolved in acetonitrile (8 mL), evaporated using a rota-vap, and rehydrated in 2 mL of HEPES to afford DiD loaded bis-F127-MA micelle solution (5%, *w/v*). An equal volume of 5% DiD loaded micelle solution was mixed with 5% HASH solution to afford DiD loaded F127-HA hydrogel. To load Cy5.5-BSA, 1 mg of Cy5.5-BSA was dissolved in 5% (*w/v*) HASH solution and then mixed with bis-F127-MA micelle to obtain Cy5.5-BSA loaded hydrogel.

The release study was then performed to determine the cumulative release percentages of DiD and Cy5.5-BSA over time. Briefly, 500 μL of the hydrogel precursor solution was placed into the mold and allowed to gel. The fully cured hydrogel samples were then removed and placed in vials containing 2 mL of 1 \times PBS (10 mmol/L, pH 7.4) at 37 °C under shaking (100 rpm). At predetermined time points, release media were collected and replaced with fresh media. The concentrations of DiD and Cy5.5-BSA in the release samples were then analyzed by fluorescence spectrometry using a Varioskan flash multimode microplate reader (Thermo Fisher Scientific, USA). The cumulative release percentage was then calculated, and the release profiles of DiD and Cy5.5-BSA were analyzed using mathematical models as previously described²⁸.

2.5. *In vivo* release of DiD and Cy5.5-BSA

Wild-type male BALB/c mice (6–8 weeks old, 18–22 g) were provided by the Laboratory Animal Center of Sichuan University (Chengdu, China). All animal protocols and studies were approved by the Ethics Committee of Sichuan University and performed per university guidelines. To conduct local injection,

15 μL of hydrogel precursor solution was injected into the renal capsule of the left kidney of each mouse. Following administration, mice were imaged using IVIS Spectrum Imaging System (PerkinElmer, USA) on Days 1, 3, 7 and then weekly until Day 21. Fluorescence intensity (Cy5.5-BSA: $\lambda_{\text{ex}}/\lambda_{\text{em}} = 620/710$ nm; DiD: $\lambda_{\text{ex}}/\lambda_{\text{em}} = 644/665$ nm) was semi-quantitatively analyzed and normalized to the peak intensity of each mouse as previously reported²⁹.

2.6. Therapeutic efficacy in unilateral ureteral obstruction (UUO) mice

Wild-type male BALB/c mice were used to establish mouse UUO model by ligation of the left ureter as previously reported³⁰. Immediately after ligation, mice in six groups were treated accordingly: i) sham operation group (sham); ii) UUO group with no treatment (UUO); iii) UUO group followed by intravenous injection of CLT solution (UUO + CLTs, 3 mg/kg \times 4 times); iv) UUO followed by a single injection of F127-HA hydrogel into the renal capsule (15 μL blank hydrogel); v) UUO followed by a single injection of F127-HA hydrogel containing CLT (3 mg/kg CLT, 15 μL); vi) UUO followed by a single injection of F127-HA hydrogel containing anti-TGF- β 1 antibody (100 μg). To evaluate the therapeutic efficacy, healthy mice without any operation or treatment served as negative control. Above hydrogel precursor solutions containing different treatments were locally injected at the renal capsule of the affected kidney immediately after the initial UUO procedure^{31,32}. Mice were sacrificed on Days 7, 14, and 21 following the initial UUO operation. All animals were handled in compliance with internal guidelines, and above animal protocols and operations were approved by the Ethics Committee of Sichuan University, China.

2.7. Immunofluorescence staining of macrophages

Paraffin-embedded kidney sections were dewaxed with a gradient ethanol solution, then antigen-repaired with EDTA antigen repair solution, and blocked with BSA for 30 min. Next, the primary antibodies were incubated in a wet box at 4 $^{\circ}\text{C}$ overnight followed by secondary antibody incubation at room temperature for about 50 min in the dark. DAPI was used to counterstain nuclei for 10 min. The following primary antibodies were used: rat polyclonal F4/80 antibody (1:100 dilution, Abcam, USA), rabbit polyclonal CD206 antibody (1:100 dilution, Abcam, USA) and rabbit polyclonal iNOS antibody (1:100 dilution, Abcam, USA) to label anti-inflammatory (M2) and pro-inflammatory (M1) macrophages, respectively. The secondary antibodies included: Cy3 conjugated goat anti-rabbit IgG (catalog number GB21303, 1:300 dilution, Servicebio, China), and Alexa Fluor[®] 488-conjugated AffiniPure goat anti-rabbit IgG (catalog number GB25303, 1:400 dilution, Servicebio, China). Fluorescence images were taken on a confocal microscope (LSM 800, Carl Zeiss, Jena, Germany) obtaining 18 images per section. As previously mentioned³³, the average fluorescence intensity was quantitated by ImageJ (NIH, Bethesda, USA). The mean gray value (MOD) of positive staining in the visual field of each slide was calculated respectively.

2.8. Immunostaining and histological analysis

To evaluate the *in vivo* efficacy and systemic toxicity, standard hematoxylin and eosin (H&E) staining was conducted on kidney and vital organ sections. To evaluate cell apoptosis, *in situ* cell

death detection kit-POD (Roche, Switzerland) was used per manufacturer's instruction, and the cell nuclei were counterstained by hematoxylin. Next, fibrosis was evaluated following Masson's trichrome staining (Servicebio, China). Apoptotic cells were analyzed at 40 \times magnification, and the fibrotic area was semi-quantitatively analyzed for trichrome staining using Image-Pro Plus software (Media Cybernetics, USA).

To further characterize fibrosis and inflammatory cytokine levels of the affected kidney, immunostaining was performed on kidney sections using primary antibodies for α -smooth muscle actin (α -SMA, 1:100 dilution, Abcam, USA), cluster of differentiation 68 (CD68, 1:80 dilution, Abcam, USA), Collagen I (1:100 dilution, Abcam, USA), tumor necrosis factor α (TNF- α , 1:120 dilution, Abcam, USA), interleukin 6 (IL-6, 1:100 dilution, Abcam, USA), and interleukin 1 β (IL-1 β , 1:80 dilution, Affinity, USA) with biotinylated goat anti-rabbit IgG (Zhongshan Jinqiao Biotechnology, Beijing, China) as the secondary antibody. Representative images were obtained using an inverted microscope (Leica, Germany). The levels of collagen deposition and inflammatory cytokines such as TNF- α , IL-6, and IL-1 β were semi-quantitatively analyzed at 40 \times magnification using Image-Pro Plus software (Media Cybernetics, USA).

2.9. Statistics

Data were presented as mean \pm standard deviation (SD) of minimum three replicates unless otherwise indicated. Comparisons among multiple groups were conducted by one-way ANOVA followed by a Tukey *post hoc* analysis using GraphPad Prism 5.0 (La Jolla, CA, USA). *P*-values of less than 0.05 were considered statistically different.

3. Results and discussions

3.1. Synthesis of hydrogel precursors

Triblock Pluronics[®] (PEO-PPO-PEO) are commercially available amphiphiles, which undergo self-assembly into nanoscale micelles thus being a good pharmaceutical excipient for solubilizing hydrophobic drugs. Among commercially available Pluronics, F127 (Mw 12,600 Da) was selected due to its suitable hydrophilic-lipophilic balance value, which has previously been proven to assemble into micelles with an average size of around 30 nm³⁴. Thiolated HA (HASH) and bismethacrylate Pluronic F127 (bis-F127-MA) were synthesized using established methods (Schemes S1 and S2)^{35–37}. The chemical structures of HASH and Bis-F127-MA were validated by magnetic resonance spectroscopy (Figs. S1 and S2). In the following study, we would explore a simple approach utilizing a triblock Pluronic-based micelle with HA hydrogel for the controlled and prolonged delivery of both small molecule and macromolecule drugs. Using shell functionalized micellar particles as the hydrogel crosslinkers, efficient *in situ* gelation are expected to be achieved under physiological conditions which then act as a drug-containing depot to provide long-term release *in vivo*.

3.2. Gelation study and characterizations

To prepare Pluronic micelles, a thin film evaporation and dispersion method was adopted, and bis-F127-MA was proven to self-assemble into near spherical particles in the aqueous solution with

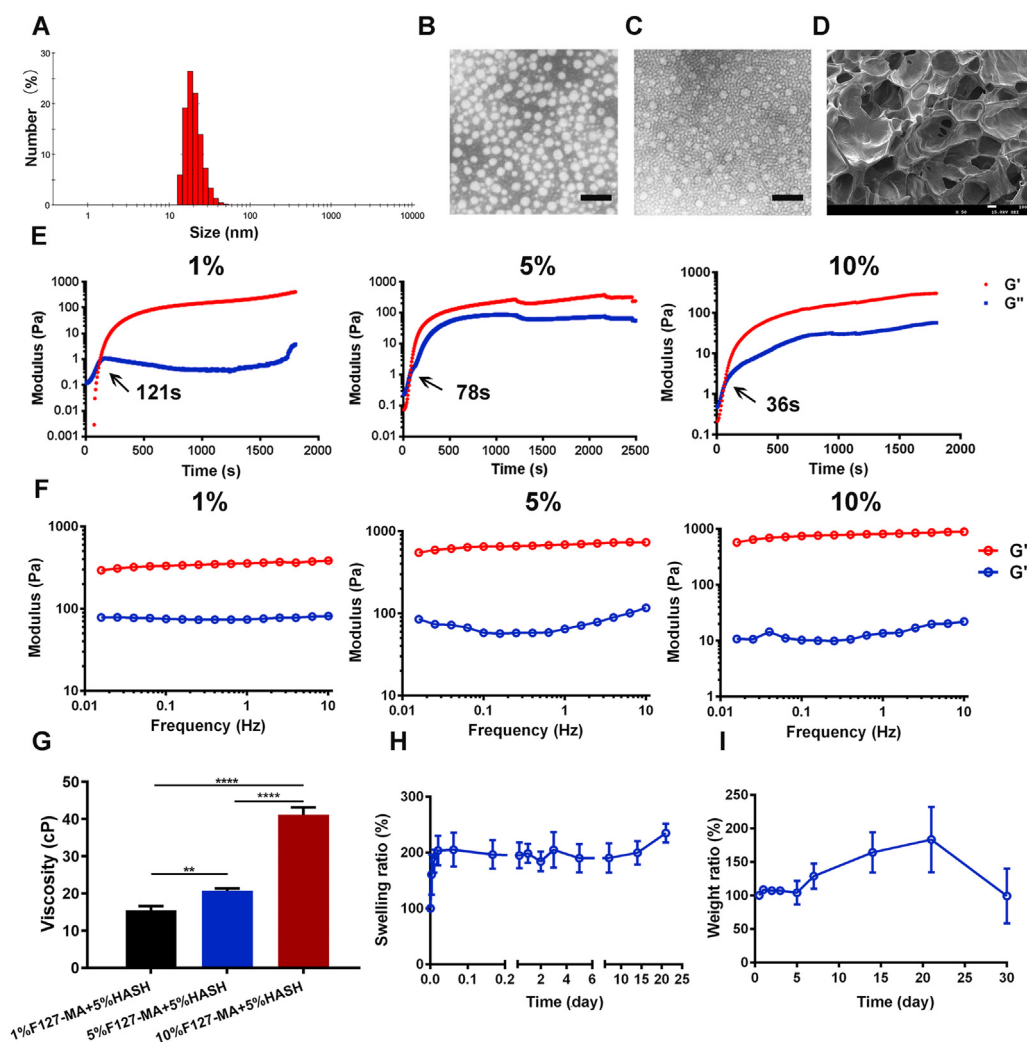


Figure 1 Physicochemical characterizations of bis-F127-MA micelles crosslinked HA hydrogels. Size distribution profile of bis-F127-MA micelles determined by dynamic light scattering (A). Representative TEM images of bis-F127-MA micelles (B), and F127-HA hydrogel (C). Representative SEM image of lyophilized F127-HA hydrogel (D). Scale bars = 100 nm. Rheological characterization of F127-HA hydrogels via dynamic time sweep (E) and frequency sweep (F) tests. The viscosities (G), swelling (H) and degradation (I) over time profiles of F127-HA hydrogels. Data represent mean \pm SD ($n = 3$). * $P < 0.05$, ** $P < 0.01$ and *** $P < 0.001$.

an average size of about 35.6 nm (PDI = 0.168 ± 0.02), and a zeta potential of -0.13 ± 0.011 mV (Fig. 1A and B), which are consistent with the size and zeta potential of Pluronic F127 micelles without any chemical modification²⁷. The encapsulation efficiency for various hydrophobic small molecules in bis-F127-MA micelles remained above 90% with loading capacities of around 2% (Supporting Information Table S1) indicating the suitability and feasibility of bis-F127-MA micelles for drug encapsulation and solubilization.

To perform gelation study, bis-F127-MA micelles were synthesized as aforementioned and dispersed in HEPES (0.5 mmol/L, pH 8.0) at polymer concentrations of 1%, 5% and 10% (w/v). Meanwhile, HASH was dissolved in ddH₂O at concentrations of 1%, 5% and 10% (w/v). Bis-F127-MA micelle dispersions and HASH were then mixed and achieved complete gelation within 5 min at 37 °C (Supporting Information Fig. S4). To examine the micelle structure within the fully cured hydrogel network, equal volumes of bis-F127-MA micelles and HASH solution were well mixed and allowed to form a thin hydrogel layer over the

transmission electron microscopy (TEM) grids. The TEM image showed that bis-F127-MA micelles uniformly distributed within the hydrogel network and maintained their near spherical morphology similar to bis-F127-MA micelle suspensions (Fig. 1C). After lyophilization, F127-HA hydrogel network displayed the typical porous microstructure under SEM (Fig. 1D), the pore size of which could be modulated by varying the total polymer concentration or crosslinking density.

Next, the gelation kinetics of the F127-HA hydrogels was characterized by strain oscillatory shear experiments. Per the time sweep test, all three formulations achieved rapid sol–gel transition within 5 min (Fig. 1E). Also, the gelation time gradually decreased with increasing concentrations of precursor solutions (Fig. 1E). Consistent with previous findings, changing the concentration of hydrogel precursors may help modulate the rate of crosslinking and the gelation time^{35,38}. Moreover, dynamic modulus measurements were employed to gain insights into the viscoelastic properties of fully cured hydrogels. All three formulations showed G' (storage modulus) $>$ G'' (loss modulus),

indicating an elastic nature of fully cured F127-HA hydrogels. G' values have also been shown to increase with increasing polymer concentrations (Fig. 1F). To determine the injectability properties, the viscosity of hydrogel precursor solutions was determined using a standard viscometer, and all three formulations displayed viscosity values below 50 cP, which indicates the hydrogel precursor solutions can easily go through 22-gauge needles (Fig. 1G).

Per the dynamic equilibrium swelling study, 5% hydrogel underwent rapid swelling in PBS reaching the equilibrium swelling state in about 20 min (Fig. 1H), and its equilibrium swelling rate (ESR) reached 200%, presumably due to the loose and porous structure of hyaluronan-based networks. Moreover, the 5% hydrogels started to lose their bulk integrity over time as observed by mass loss after 20 days (Fig. 1I).

Another unique feature of the F127-HA hydrogel is its capacity to load poorly water-soluble small molecule drugs and to achieve controlled and prolonged release. Interestingly, without encapsulating in the bis-F127-MA micellar core prior to gelation, physically mixed dexamethasone (DEX) in F127-HA hydrogel displayed an opaque feature which appeared to be suspended in the hydrogel matrix (Supporting Information

Fig. S3). In contrast, when DEX was encapsulated in bis-F127-MA micelles prior to forming crosslinked hydrogel, the DEX loaded F127-HA hydrogel displayed a transparent feature (Fig. S3), indicating the extraordinary solubilizing capacity of Pluronic F127 micelles. However, the SEM images did not reveal much variations in the microstructure of these two hydrogel formulations both showing a porous structure after freeze-drying (Fig. S3).

3.3. *In vitro* and *in vivo* release studies

According to a preliminary 14 d release study, CLT and Cy5.5-BSA from F127-HA hydrogel hybrid showed a rapid initial burst with over 60% cumulative release within the first 24 h followed by gradually increasing cumulative release for up to 14 days (Supporting Information Fig. S4). The rapid initial burst release *in vitro* is likely due to the rapid swelling effect of the hydrogel hybrid as demonstrated in the previous section; however, when in the *in vivo* environment, the hydrogel hybrid may not undergo such rapid swelling due to the limited body fluid around, which may result in reduced initial burst.

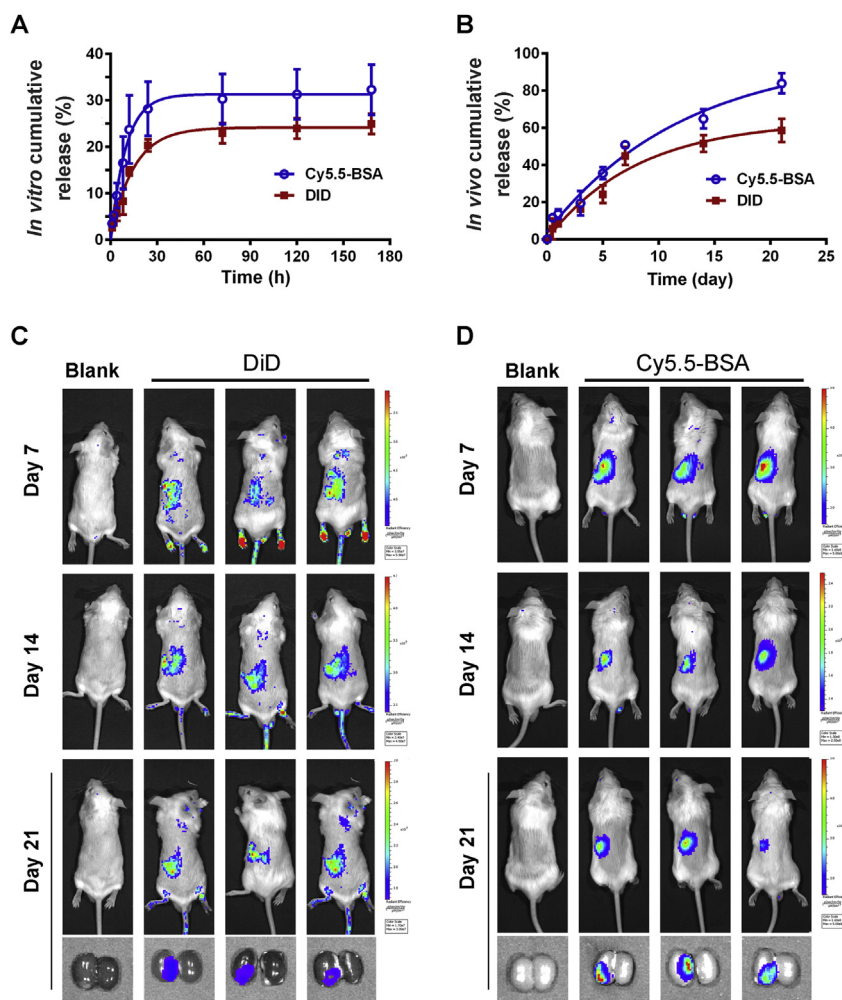


Figure 2 Release profiles of F127-HA hydrogels. *In vitro* release profiles of DiD and Cy5.5-BSA from F127-HA hydrogels (A). Semi-quantitative *in vivo* release profiles of DiD and Cy5.5-BSA from F127-HA hydrogels (B). Representative *in vivo* optical images of DiD (C) and Cy5.5-BSA (D) loaded hydrogel following localized injection in healthy mice. Data represent mean \pm SD ($n = 3$).

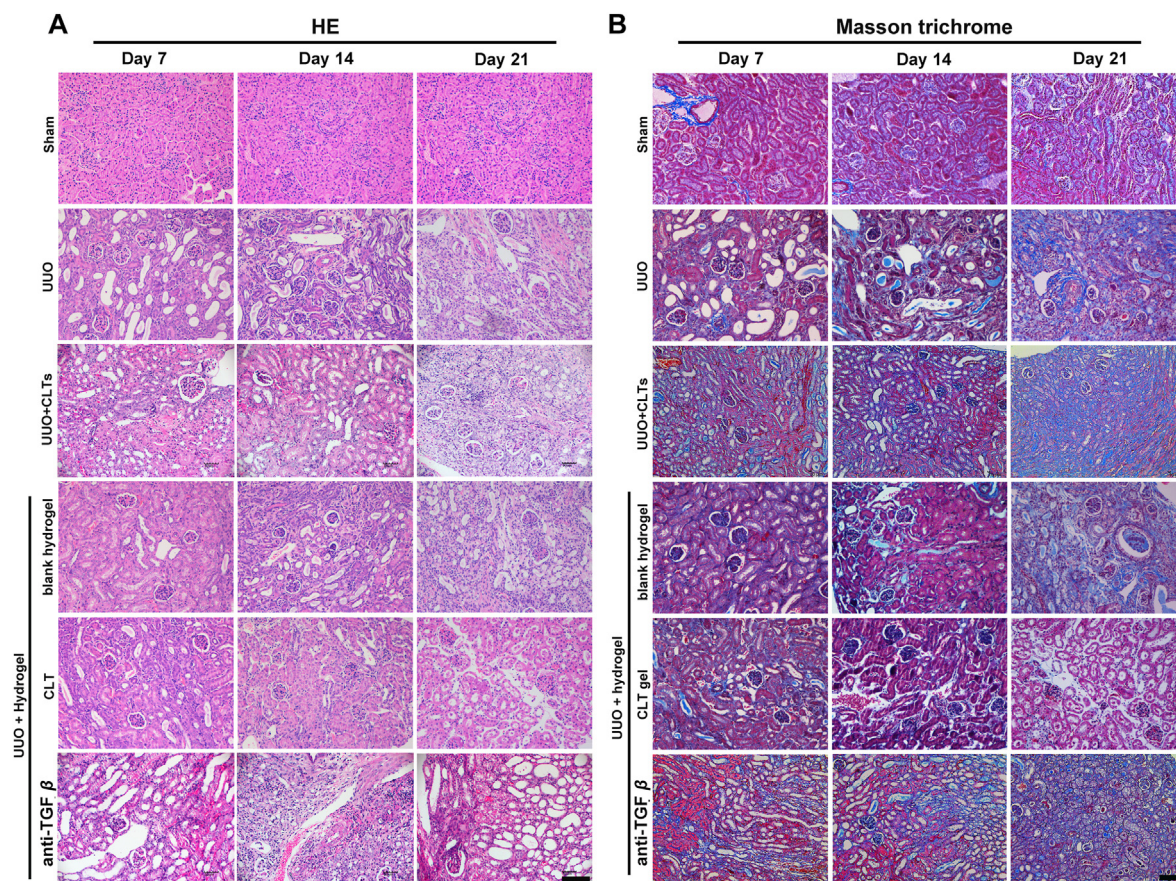


Figure 3 Representative images of the affected kidney sections by H&E (A) and Masson's trichrome staining (B). Scale bars = 100 μ m.

To gain connection between the *in vitro* and *in vivo* release, a near infrared hydrophobic probe DiD and Cy5.5-BSA were selected as two model solutes in the following release studies. DiD was encapsulated in the hydrophobic core of the bis-F127-MA micelles and further afforded the DiD loaded F127-HA hydrogel. Meanwhile, Cy5.5-BSA was synthesized, mixed with HASH solution, and then crosslinked by bis-F127-MA micelles. Both DiD and Cy5.5-BSA achieved continuous release for up to 7 days *in vitro* (Fig. 2A), while *in vivo*, both solutes showed continuous release for up to 21 days with a gradual decay of the fluorescence intensity over time (Fig. 2B–D). Consistently, Cy5.5-BSA showed more rapid and higher cumulative release than DiD from F127-HA hydrogels at all given time points both *in vitro* and *in vivo* (Fig. 2A and B), indicating the release of Cy5.5-BSA was mainly driven by diffusion and polymer relaxation. In contrast, the lower cumulative release of DiD at each given time point from *in vitro* and *in vivo* studies was likely due to the encapsulation in the micellar core of the bis-F127-MA micelles thus presenting an additional barrier for solute diffusion other than HA scaffolds. Additionally, the solutions of both DiD and Cy5.5-BSA following local injection in the kidney were shown to retain at the injection site for about three days (Supporting Information Fig. S5), which further supports that localized delivery *via* hydrogel contributes to the prolonged release *in vivo*. Per mathematical modelling analysis, the Ritger–Peppas equation showed the best correlation for both DiD and Cy5.5-BSA from *in vivo* release profiles, which indicates that the releases of both small molecule drugs and bio-macromolecules out of the F127-HA hydrogel hybrid were mostly

non-Fickian diffusion driven (Supporting Information Table S2). Also, the release was proportional to time and partially dependent on the swelling and relaxation of polymer chains within the hydrogel.

3.4. *In vivo* gelation and biocompatibility

To explore the injectability and gelation *in vivo*, DiD-loaded hydrogel precursor solutions were injected subcutaneously in mice. Complete gelation was observed at 5 min post injection (Supporting Information Fig. S6), which suggests that the F127-HA hydrogel be suitable for localized injection in the kidney.

Next, to evaluate the injectability and gelation in kidney, 15 μ L of hydrogel precursor solution containing either DiD or Cy5.5-BSA was locally injected in the kidney of healthy mouse. After injection, mice were subjected to *in vivo* imaging at predetermined time points. As shown in the representative images, the injected hydrogel was well retained at the injection site in the affected kidney for up to three weeks (Fig. 2C and D), which will likely result in localized and prolonged drug release.

Per histological analysis, the injection of the F127-HA hydrogel did not invoke any obvious tissue toxicity or inflammatory cell infiltration in the affected kidney for up to 21 days (Supporting Information Fig. S7). In addition, compared with the normal group, the implantation of the hydrogel containing near infrared dyes DiD or Cy5.5-BSA will not have any influence on the renal function indexes (Supporting Information Fig. S8),

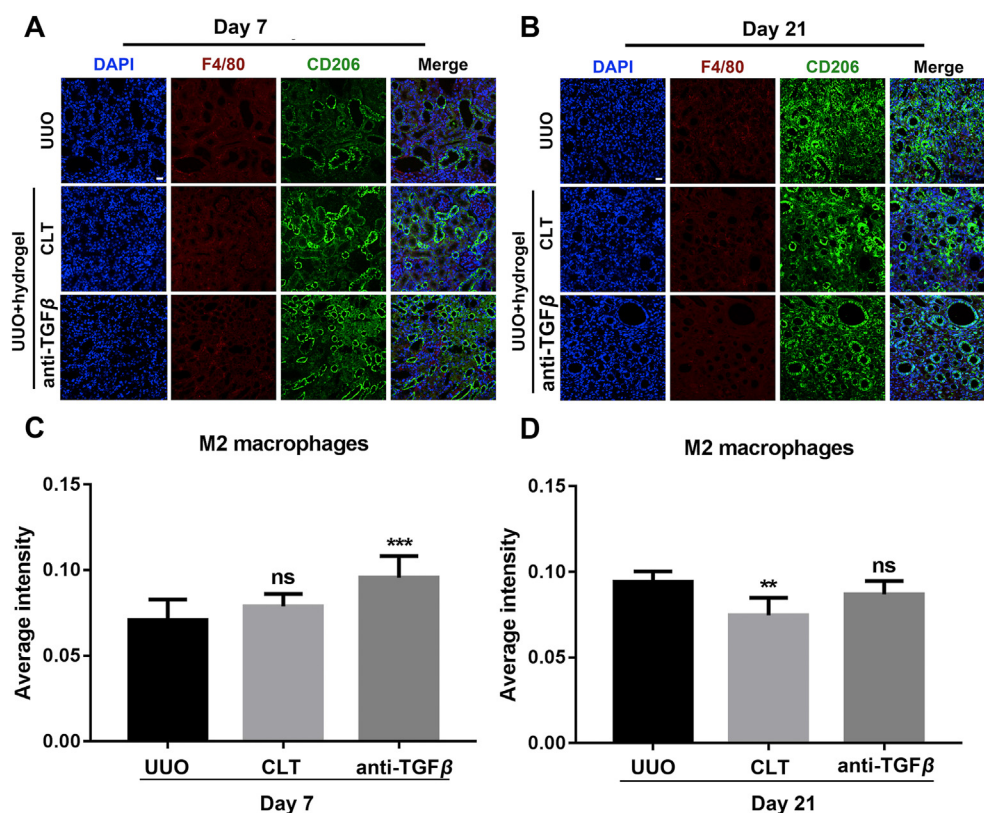


Figure 4 Anti-inflammatory (M2-like) macrophage profiles on histological injury and development of renal fibrosis in UUO mice. Representative immunofluorescence staining images of CD206/F4/80 on the affected kidney sections at Day 7 (A) and Day 21 (B). Scale bars = 20 μ m. Macrophage distribution was assessed semi-quantitatively by fluorescence counting (C) and (D). Each evaluation represents the mean \pm SD ($n = 6$). ** $P < 0.01$, *** $P < 0.001$ vs. UUO group. ns, not significant.

indicating remarkable biocompatibility of the F127-HA hydrogel hybrid *in vivo*.

3.5. Mice UUO model and therapeutic efficacy

After confirming the biocompatibility of F127-HA hydrogels, a UUO mice model was established to evaluate the anti-fibrosis effect of the proposed localized therapy^{31,32,39,40}. CLT and anti-TGF β 1 antibody were selected as model therapeutics to explore the therapeutic efficacy of localized drug delivery in anti-fibrosis study *in vivo*. CLT was successfully encapsulated within the core of bis-F127-MA micelles to afford CLT loaded F127-HA hydrogel, while anti-TGF β 1 antibody was uniformly dispersed in the HASH solution and further crosslinked by bis-F127-MA micelles to afford anti-TGF β 1 antibody loaded F127-HA hydrogel. Treatment was initiated immediately post UUO surgery, the renal tissues after treatments were collected on Days 7, 14, and 21 for immunohistochemical analysis (Scheme 2).

Compared with sham control, the UUO group showed tubular atrophy and extensive inflammatory cell infiltration over time (Fig. 3A). Compared with UUO group, all treatment groups demonstrated positive therapeutic efficacy with decreased inflammatory cell infiltration and reduced morphological changes (Fig. 3A). Also, the systemic toxicity of CLT following intravenous injection was greatly relieved by the localized therapy as indicated by reduced cardiotoxicity in the CLT hydrogel group

(Fig. S8), which demonstrates the great potential of delivering anti-inflammatory drugs locally instead of systemically.

To evaluate fibrosis, the Masson's trichrome and α -SMA staining was performed and the results further demonstrated an obvious increase in the fibrosis area of the UUO group over time (Fig. 3B, Supporting Information Figs. S10 and S11). At Day 21, the fibrosis area showed progressive and significant increases for the untreated UUO and the group treated with either F127-HA hydrogel alone or CLT solution alone, indicating CLT solution following systemic administration did not show efficacy against renal fibrosis (Fig. 3B and Fig. S10). As a comparison, F127-HA hydrogel containing either CLT or anti-TGF β 1 antibody showed significantly reduced fibrotic areas compared with untreated UUO at day 21 (Fig. 3B and Fig. S11). Consistently, collagen I deposition was greatly downregulated in F127-HA/CLT or F127-HA/anti-TGF β 1 groups on Day 21 (Supporting Information Fig. S12). On Day 21, macrophage infiltration was significantly reduced in the groups treated with F127-HA hydrogel containing either CLT or anti-TGF β 1 antibody as compared to the F127-HA hydrogel only group (Fig. S10 and Supporting Information Fig. S13).

At present, TGF- β 1 is recognized as one of the key regulatory factors contributing to the deposition of extracellular matrix (ECM) in the fibrotic region^{41,42}. Therapeutics commonly used for the treatment of renal interstitial fibrosis include anti-TGF β 1 antibody^{43–45}, anti-fibrosis cytokine^{46–48}, and various kinase inhibitors^{13,15,16,29,49}. As expected, anti-TGF β 1 loaded F127-HA

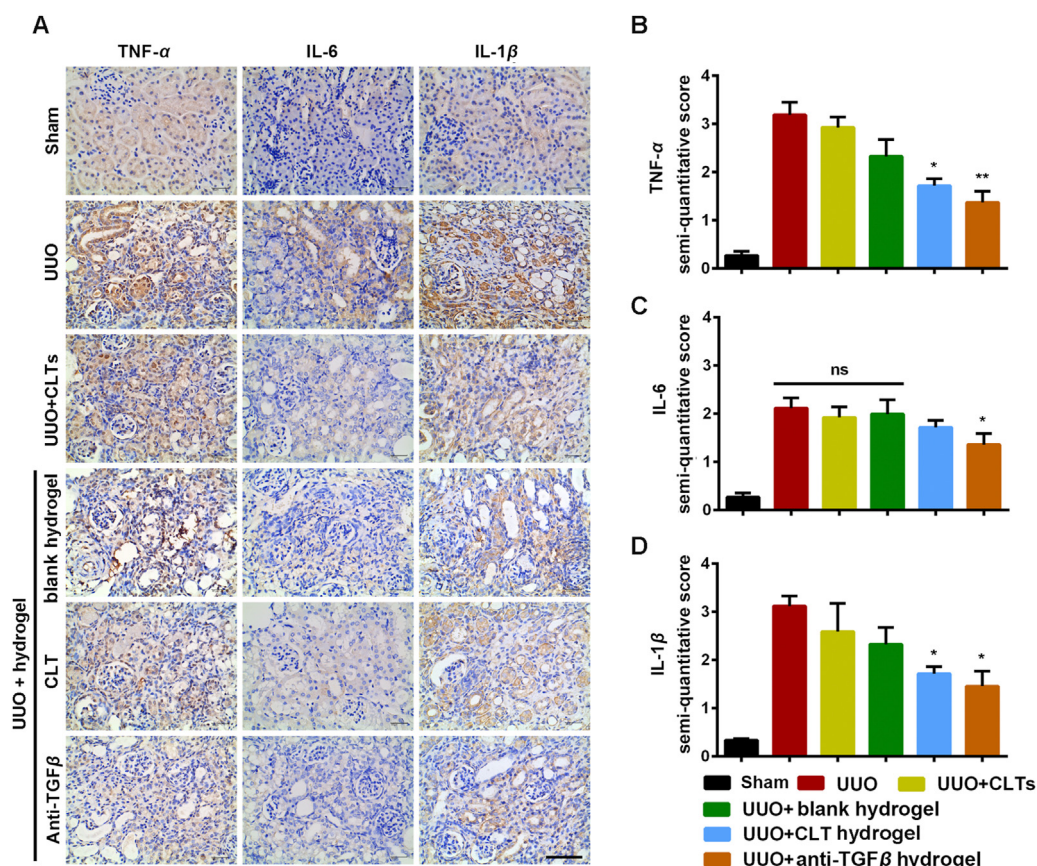


Figure 5 Representative images of affected kidneys by immunostaining of TNF- α , IL-6 and IL-1 β at 21 days post unilateral ureteral ligation (A). Semi-quantitative analysis of the levels of TNF- α (B), IL-6 (C) and IL-1 β (D) following different treatments. Scale bar = 100 μ m. Data are mean \pm SD ($n = 3$). * $P < 0.05$ vs. UUO group.

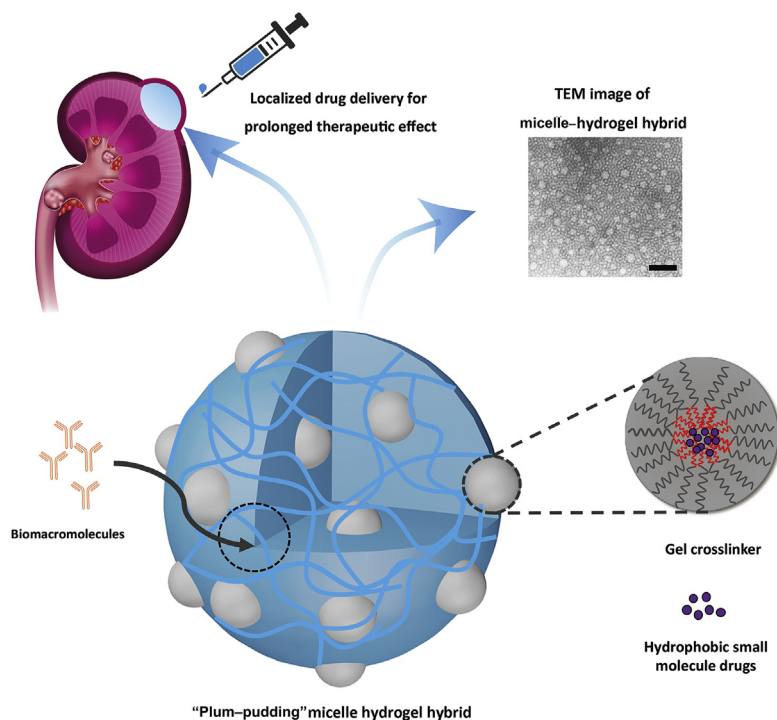
hydrogel showed remarkable efficacy against renal fibrosis (Fig. 3).

3.6. Localized treatments differentially modulate macrophage plasticity

Different subtypes of macrophages have been found to play critical roles in many human diseases or experimental disease models such as cancer, inflammation, and fibrosis^{50–55}. Pro-inflammatory macrophages (M1-like) produce pro-inflammatory cytokines, *e.g.*, IL-1, TNF- α and macrophage migration inhibitory factor, thus causing acute tissue injury, while anti-inflammatory or pro-fibrotic macrophages (M2-like) promote fibrosis *via* multiple mechanisms⁵⁶.

To elucidate the role of macrophages during the progression of fibrosis in UUO model, the plasticity patterns of renal macrophages in the affected kidney after unilateral ureteral ligation were elucidated *via* immunofluorescence staining. Interestingly, the percentage of M1-like macrophage labelled by iNOS was found to be dramatically higher than that of anti-inflammatory M2-like macrophages labelled by CD206 within the first five days post ligation, suggesting acute inflammatory responses in UUO mice (Supporting Information Fig. S14). About 7 days post ligation,

increases in the percentage of M2-like macrophages were observed in both localized treatment groups, *i.e.*, CLT or anti-TGF β hydrogel, indicating that the immunomodulatory effect kicked in by accumulating a large number of M2-like macrophages to suppress inflammation (Fig. 4A and C). Specifically, localized anti-TGF β hydrogel showed a more profound impact on upregulating the level of M2-like macrophages on day 7 post ligation (Fig. 4A and C). Compared with the 7-day results, M2-like macrophages were significantly upregulated on Day 21 in the UUO group (Fig. 4B and D), suggesting a possible correlation between the massive accumulation of M2 macrophages and the excessive deposition of ECM. This observation is consistent with literature findings that M2-like macrophages in UUO mice show pro-fibrotic effect⁵⁶. In comparison, the localized CLT or anti-TGF β 1 treatment groups showed enhanced M2-like macrophage polarization on Day 7 (Fig. 4), whereas after 21 days, localized CLT group showed significantly reduced M2-like macrophage percentage as compared to that of the UUO group ($P < 0.05$). However, localized anti-TGF β 1 treatment did not result in an obvious reduction in M2-like macrophages *versus* UUO group (Fig. 4). Taken together, these results showed correlation with Masson's trichrome staining results (Fig. 3B), which suggests renal fibrosis can be alleviated by localized CLT or anti-TGF β 1

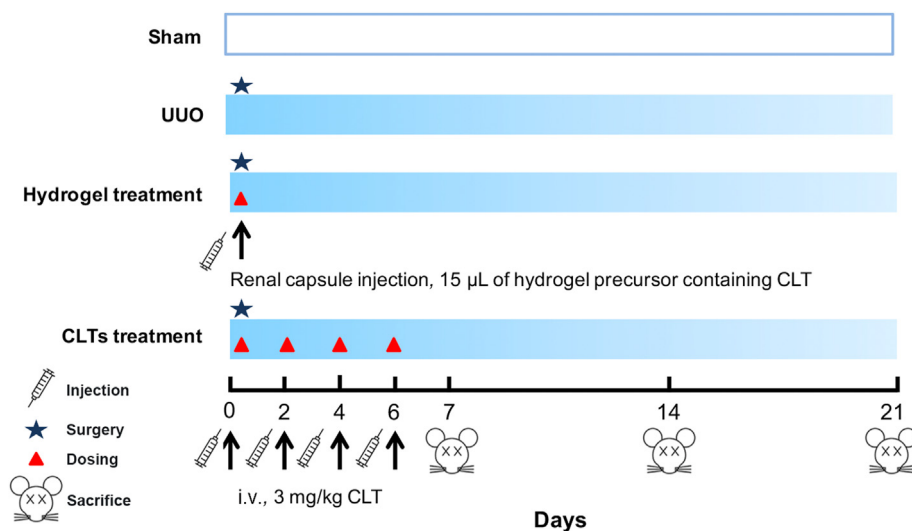


Scheme 1 Schematic representation of the “plum–pudding” system consisting of hyaluronic acid (HA) derived hydrogel crosslinked *via* self-assembled triblock micelles.

antibody treatment, possibly by inhibiting acute inflammation by upregulating M2-like macrophages in the early stage while reversing the excessive deposition of ECM by downregulating the accumulation of M2-like macrophages in the later stage. CLT and anti-TGF β antibody work as anti-fibrosis therapeutics *via* different pathways and mechanisms. Hence, localized delivery of CLT or anti-TGF β antibody appeared to differentially modulate macrophage plasticity at the different stages of UUO mice to minimize matrix deposition.

3.7. Anti-fibrosis effect via neutralizing TGF β 1 or inhibiting NF- κ B locally

Active TGF β 1 plays a critical role in activating Smad2/3 and mediating renal fibrosis, and therefore, fibrotic kidney is often associated with an upregulated level of TGF β 1^{57,58}. However, systemic administration of anti-TGF β 1 antibody may lead to various issues due to the extensive distribution of TGF β 1 in the body, which is commonly involved in various physiological



Scheme 2 UUO in BALB/c mice and dosing regimen.

pathways⁵⁹. Thus, neutralizing TGF β 1 locally at the disease site serves as a potential strategy to overcome fibrosis. To further elucidate the anti-fibrosis mechanism, we analyzed the apoptosis rate of the affected kidney sections *via* TUNEL staining, which showed downregulated apoptosis levels for localized treatment with either CLT or anti-TGF β 1 as compared to UUO group (Supporting Information Fig. S15). However, systemic administration of CLT showed no improvement in the apoptosis rate compared to UUO group (Fig. S14).

When it comes to inflammation and renal fibrosis, kidney injury induces inflammation, while unresolved inflammation may lead to fibrosis as well as end-stage renal disease⁶⁰. The activation of NF- κ B and the infiltration of macrophages and lymphocytes have been identified as the major inflammatory components⁶¹. Thus, administration of inhibitors towards NF- κ B signaling pathway may help resolve inflammation and possibly minimize fibrosis. According to our previous works and others', CLT is a well proven inhibitor for NF- κ B pathway thus showing outstanding anti-inflammatory activities in a number of diseases including acute pancreatitis⁶², rheumatoid arthritis⁶³, and glomerulonephritis²⁰. As a result, we analyzed the downstream signaling factors of NF- κ B signaling pathway including tumor necrosis factor α (TNF- α), interleukin 6 (IL-6), and interleukin 1 β (IL-1 β) (Supporting Information Fig. S16–S18). Compared with sham group, untreated UUO showed significantly upregulated levels of TNF- α , IL-6 and IL-1 β ($P < 0.05$, Fig. 5), whereas localized delivery of CLT *via* F127-HA hydrogel showed greater downregulations of the inflammatory chemokines and cytokines than systemic administration of CLT repeatedly (Fig. 5). Collectively, these results further support that the sustained release of anti-inflammation therapeutics following localized administration may greatly benefit the treatment of RIF.

4. Conclusions

In summary, an injectable triblock copolymeric micelle-crosslinked hyaluronan hydrogel hybrid offers a unique “plum-pudding” structure to deliver hydrophobic small molecules as well as biomacromolecules in a prolonged and controlled manner. Compared to existing hydrogel implants, the F127-HA micelle hydrogel hybrid was proven to solubilize poorly water-soluble drugs while achieving localized controlled drug release *in vivo*. Treatment with F127-HA hydrogel hybrid containing anti-inflammatory CLT greatly downregulated proinflammatory cytokine levels thus minimizing local inflammatory responses. The localized anti-inflammation therapy represents a viable strategy to manage chronic kidney diseases, which are proven to impact inflammation, apoptosis, and ECM deposition in UUO mice. Furthermore, delivering anti-TGF β 1 antibody locally *via* F127-HA hydrogel hybrid demonstrated great potential in the management of UUO renal fibrosis. Overall, this versatile injectable F127-HA hydrogel hybrid represents a neat and clinically relevant platform system to achieve localized therapy, which may further be explored to achieve concurrent loading and prolonged release of both small molecules and macromolecular therapeutics for other disease therapies.

Acknowledgments

This work was supported by the National Natural Science Foundation of China (81773654, 81690261, 81503018), Sichuan

Provincial Science and Technology Department (2019YJ0019, China), National Key Research and Development Plan of China (2017YFC1104601), Sichuan University Fund for Excellent Young Scholars (2017SCU04A23, China), and 111 Project (B18035, China).

Author contributions

Yao Fu was responsible for study concepts, experimental guidance, as well as funding and equipment support. Xianyan Qin and Yingying Xu carried out the experiments, generated and analyzed data, and drafted the original manuscript. Xu Zhou helped with animal studies. Tao Gong and Zhi-Rong Zhang were responsible for funding and equipment support. All of the authors have read and approved the final manuscript.

Conflicts of interest

A patent for the materials developed in this manuscript has been filed by Yao Fu and Zhi-Rong Zhang.

Appendix A. Supporting information

Supporting data to this article can be found online at <https://doi.org/10.1016/j.apsb.2020.10.016>.

References

1. Wolinsky JB, Colson YL, Grinstaff MW. Local drug delivery strategies for cancer treatment: gels, nanoparticles, polymeric films, rods, and wafers. *J Control Release* 2012;**159**:14–26.
2. During MJ, Freese A, Deutch AY, Kibat PG, Sabel BA, Langer R, et al. Biochemical and behavioral recovery in a rodent model of Parkinsons-disease following stereotaxic implantation of dopamine-containing liposomes. *Exp Neurol* 1992;**115**:193–9.
3. Uhrich KE, Cannizzaro SM, Langer RS, Shakesheff KM. Polymeric systems for controlled drug release. *Chem Rev* 1999;**99**:3181–98.
4. Brem H, Piantadosi S, Burger PC, Walker M, Selker R, Vick NA, et al. Placebo-controlled trial of safety and efficacy of intraoperative controlled delivery by biodegradable polymers of chemotherapy for recurrent gliomas. *Lancet* 1995;**345**:1008–12.
5. Mathios D, Kim JE, Mangraviti A, Phallen J, Park CK, Jackson CM, et al. Anti-PD-1 antitumor immunity is enhanced by local and abrogated by systemic chemotherapy in GBM. *Sci Transl Med* 2016;**8**:370ra180.
6. Lin CC, Metters AT. Hydrogels in controlled release formulations: network design and mathematical modeling. *Adv Drug Deliv Rev* 2006;**58**:1379–408.
7. Yu L, Ding J. Injectable hydrogels as unique biomedical materials. *Chem Soc Rev* 2008;**37**:1473–81.
8. Gu D, O'Connor AJ, Qiao GGH, Ladewig K. Hydrogels with smart systems for delivery of hydrophobic drugs. *Expert Opin Drug Deliv* 2017;**14**:879–95.
9. Li JY, Mooney DJ. Designing hydrogels for controlled drug delivery. *Nat Rev Mater* 2016;**1**:16071.
10. Nanthakumar CB, Hatley RJD, Lemma S, Gaudie J, Marshall RP, Macdonald SJF. Dissecting fibrosis: therapeutic insights from the small-molecule toolbox. *Nat Rev Drug Discov* 2015;**14**:693–720.
11. Daniels CE, Lasky JA, Limper AH, Mieras K, Gabor E, Schroeder DR, et al. Imatinib treatment for idiopathic pulmonary fibrosis randomized placebo-controlled trial results. *Am J Respir Crit Care Med* 2010;**181**:604–10.
12. Prey S, Ezzedine K, Doussau A, Grandoulier AS, Barcat D, Chatelus E, et al. Imatinib mesylate in scleroderma-associated diffuse

- skin fibrosis: a phase II multicentre randomized double-blinded controlled trial. *Br J Dermatol* 2012;**167**:1138–44.
13. Shihab FS. Do we have a pill for renal fibrosis?. *Clin J Am Soc Nephrol* 2007;**2**:876–8.
 14. Breyer MD, Susztak K. The next generation of therapeutics for chronic kidney disease. *Nat Rev Drug Discov* 2016;**15**:568–88.
 15. Mackinnon M, Shurraw S, Akbari A, Knoll GA, Jaffey J, Clark HD. Combination therapy with an angiotensin receptor blocker and an ACE Inhibitor in proteinuric renal disease: a systematic review of the efficacy and safety data. *Am J Kidney Dis* 2006;**48**:8–20.
 16. Zhang F, Liu H, Liu D, Liu Y, Li H, Tan X, et al. Effects of RAAS inhibitors in patients with kidney disease. *Curr Hypertens Rep* 2017;**19**:72.
 17. Kannaiyan R, Shanmugam MK, Sethi G. Molecular targets of celastrol derived from Thunder of God Vine: potential role in the treatment of inflammatory disorders and cancer. *Cancer Lett* 2011;**303**:9–20.
 18. Cao X, Hu Y, Luo S, Wang Y, Gong T, Sun X, et al. Neutrophil-mimicking therapeutic nanoparticles for targeted chemotherapy of pancreatic carcinoma. *Acta Pharm Sin B* 2019;**9**:575–89.
 19. Hu Y, Chen X, Xu Y, Han X, Wang M, Gong T, et al. Hierarchical assembly of hyaluronan coated albumin nanoparticles for pancreatic cancer chemioimmunotherapy. *Nanoscale* 2019;**11**:16476–87.
 20. Guo L, Luo S, Du Z, Zhou M, Li P, Fu Y, et al. Targeted delivery of celastrol to mesangial cells is effective against mesangioproliferative glomerulonephritis. *Nat Commun* 2017;**8**:878.
 21. Wang S, Liu K, Wang X, He Q, Chen X. Toxic effects of celastrol on embryonic development of zebrafish (*Danio rerio*). *Drug Chem Toxicol* 2011;**34**:61–5.
 22. Konieczny J, Jantas D, Lenda T, Domin H, Czarnecka A, Kuter K, et al. Lack of neuroprotective effect of celastrol under conditions of proteasome inhibition by lactacystin in *in vitro* and *in vivo* studies: implications for Parkinson's disease. *Neurotox Res* 2014;**26**:255–73.
 23. Lopez-Hernandez FJ, Lopez-Novoa JM. Role of TGF-beta in chronic kidney disease: an integration of tubular, glomerular and vascular effects. *Cell Tissue Res* 2012;**347**:141–54.
 24. Qin X, Qiao W, Wang Y, Li T, Li X, Gong T, et al. An extracellular matrix-mimicking hydrogel for full thickness wound healing in diabetic mice. *Macromol Biosci* 2018;**18**:1800047.
 25. Dong D, Li J, Cui M, Wang J, Zhou Y, Luo L, et al. *In situ* "clickable" zwitterionic starch-based hydrogel for 3D cell encapsulation. *ACS Appl Mater Interfaces* 2016;**8**:4442–55.
 26. Long D, Gong T, Zhang Z, Ding R, Fu Y. Preparation and evaluation of a phospholipid-based injectable gel for the long term delivery of leuprolide acetate. *Acta Pharm Sin B* 2016;**6**:329–35.
 27. Grigolo B, Lisignoli G, Piacentini A, Fiorini M, Gobbi P, Mazzotti G, et al. Evidence for redifferentiation of human chondrocytes grown on a hyaluronan-based biomaterial (HYAFF (R) 11): molecular, immunohistochemical and ultrastructural analysis. *Biomaterials* 2002;**23**:1187–95.
 28. Cao X, Luo J, Gong T, Zhang ZR, Sun X, Fu Y. Coencapsulated doxorubicin and bromotetrandrine lipid nanoemulsions in reversing multidrug resistance in breast cancer *in vitro* and *in vivo*. *Mol Pharm* 2015;**12**:274–86.
 29. Burdick JA, Mason MN, Hinman AD, Thorne K, Anseth KS. Delivery of osteoinductive growth factors from degradable PEG hydrogels influences osteoblast differentiation and mineralization. *J Control Release* 2002;**83**:53–63.
 30. Lamb CR, Cortellini S, Halfacree Z. Ultrasonography in the diagnosis and management of cats with ureteral obstruction. *J Feline Med Surg* 2018;**20**:15–22.
 31. Rodell CB, Rai R, Faubel S, Burdick JA, Soranno DE. Local immunotherapy via delivery of interleukin-10 and transforming growth factor beta antagonist for treatment of chronic kidney disease. *J Control Release* 2015;**206**:131–9.
 32. Soranno DE, Rodell CB, Altmann C, Duplantis J, Andres-Hernando A, Burdick JA, et al. Delivery of interleukin-10 via injectable hydrogels improves renal outcomes and reduces systemic inflammation following ischemic acute kidney injury in mice. *Am J Physiol Renal Physiol* 2016;**311**:F362–72.
 33. Xu Y, Qin S, Niu Y, Gong T, Zhang Z, Fu Y. Effect of fluid shear stress on the internalization of kidney-targeted delivery systems in renal tubular epithelial cells. *Acta Pharm Sin B* 2020;**10**:680–92.
 34. Cao X, Zhou X, Wang Y, Gong T, Zhang Z-R, Liu R, et al. Diblock- and triblock-copolymer based mixed micelles with high tumor penetration *in vitro* and *in vivo*. *J Mater Chem B* 2016;**4**:3216–24.
 35. Zhou X, Qin X, Gong T, Zhang Z-R, Fu Y. D-Fructose modification enhanced internalization of mixed micelles in breast cancer cells via GLUT5 transporters. *Macromol Biosci* 2017;**17**:1600529.
 36. Revzin A, Russell RJ, Yadavalli VK, Koh WG, Deister C, Hile DD, et al. Fabrication of poly(ethylene glycol) hydrogel microstructures using photolithography. *Langmuir* 2001;**17**:5440–7.
 37. Fu Y, Kao WJ. In situ forming poly(ethylene glycol)-based hydrogels via thiol-maleimide Michael-type addition. *J Biomed Mater Res Part A* 2011;**98A**:201–11.
 38. Fu Y, Xu K, Zheng X, Giacomini AJ, Mix AW, Kao WJ. 3D cell entrapment in crosslinked thiolated gelatin-poly(ethylene glycol) diacrylate hydrogels. *Biomaterials* 2012;**33**:48–58.
 39. Wang D, Xiong M, Chen Ca, Du L, Liu Z, Shi Y, et al. Legumain, an asparaginyl endopeptidase, mediates the effect of M2 macrophages on attenuating renal interstitial fibrosis in obstructive nephropathy. *Kidney Int* 2018;**94**:91–101.
 40. Soranno DE, Lu HD, Weber HM, Rai R, Burdick JA. Immunotherapy with injectable hydrogels to treat obstructive nephropathy. *J Biomed Mater Res Part A* 2014;**102**:2173–80.
 41. Hinz B. The extracellular matrix and transforming growth factor-beta 1: tale of a strained relationship. *Matrix Biol* 2015;**47**:54–65.
 42. Nastase MV, Zeng-Brouwers J, Wygrecka M, Schaefer L. Targeting renal fibrosis: mechanisms and drug delivery systems. *Adv Drug Deliv Rev* 2018;**129**:295–307.
 43. Ling H, Li XM, Jha S, Wang W, Karetskaya L, Pratt B, et al. Therapeutic role of TGF-beta-neutralizing antibody in mouse cyclosporin a nephropathy: morphologic improvement associated with functional preservation. *J Am Soc Nephrol* 2003;**14**:377–88.
 44. Ma LJ, Jha S, Ling H, Pozzi A, Ledbetter S, Fogo AB. Divergent effects of low versus high dose anti-TGF-beta antibody in puromycin aminonucleoside nephropathy in rats. *Kidney Int* 2004;**65**:106–15.
 45. Miyajima A, Chen J, Lawrence C, Ledbetter S, Soslow RA, Stern J, et al. Antibody to transforming growth factor-beta ameliorates tubular apoptosis in unilateral ureteral obstruction. *Kidney Int* 2000;**58**:2301–13.
 46. Yang JW, Dai CS, Liu YH. A novel mechanism by which hepatocyte growth factor blocks tubular epithelial to mesenchymal transition. *J Am Soc Nephrol* 2005;**16**:68–78.
 47. Zeisberg M. Bone morphogenic protein-7 and the kidney: current concepts and open questions. *Nephrol Dial Transplant* 2006;**21**:568–73.
 48. Yu MA, Shin KS, Kim JH, Kim YI, Chung SS, Park SH, et al. HGF and BMP-7 ameliorate high glucose-induced epithelial-to-mesenchymal transition of peritoneal mesothelium. *J Am Soc Nephrol* 2009;**20**:567–81.
 49. Breyer MD, Susztak K. The next generation of therapeutics for chronic kidney disease. *Nat Rev Drug Discov* 2016;**15**:568–88.
 50. Engel JE, Chade AR. Macrophage polarization in chronic kidney disease: a balancing act between renal recovery and decline?. *Am J Physiol Renal Physiol* 2019;**317**:F1409–13.
 51. Ruffell B, Affara NI, Coussens LM. Differential macrophage programming in the tumor microenvironment. *Trends Immunol* 2012;**33**:119–26.
 52. Tacke F, Zimmermann HW. Macrophage heterogeneity in liver injury and fibrosis. *J Hepatol* 2014;**60**:1090–6.
 53. Benoit M, Desnues B, Mege JL. Macrophage polarization in bacterial infections. *J Immunol* 2008;**181**:3733–9.
 54. Mantovani A, Biswas SK, Galdiero MR, Sica A, Locati M. Macrophage plasticity and polarization in tissue repair and remodelling. *Trends Immunol* 2013;**229**:176–85.
 55. Olefsky JM, Glass CK. Macrophages, inflammation, and insulin resistance. *Annu Rev Physiol* 2010;**72**:219–46.

56. Nikolic-Paterson DJ, Wang S, Lan HY. Macrophages promote renal fibrosis through direct and indirect mechanisms. *Kidney Int Suppl* 2014;**4**:34–8.
57. Munoz-Felix JM, Gonzalez-Nunez M, Martinez-Salgado C, Lopez-Novoa JM. TGF-beta/BMP proteins as therapeutic targets in renal fibrosis. Where have we arrived after 25 years of trials and tribulations?. *Pharmacol Ther* 2015;**156**:44–58.
58. Lan HY. Diverse roles of TGF-beta/smads in renal fibrosis and inflammation. *Int J Biol Sci* 2011;**7**:1056–67.
59. Meng XM, Nikolic-Paterson DJ, Lan HY. TGF-beta: the master regulator of fibrosis. *Nat Rev Nephrol* 2016;**12**:325–38.
60. Meng XM, Nikolic-Paterson DJ, Lan HY. Inflammatory processes in renal fibrosis. *Nat Rev Nephrol* 2014;**10**:493–503.
61. Miguel Lopez-Novoa J, Angela Nieto M. Inflammation and EMT: an alliance towards organ fibrosis and cancer progression. *EMBO Mol Med* 2009;**1**:303–14.
62. Zhou X, Yu R, Cao X, Zhang ZR, Deng L. Bio-mimicking nanoparticles for targeted therapy of malignant melanoma. *J Biomed Nanotechnol* 2019;**15**:993–1004.
63. Gong T, Zhang P, Deng C, Xiao Y, Gong T, Zhang Z. An effective and safe treatment strategy for rheumatoid arthritis based on human serum albumin and Kolliphor (R) HS 15. *Nanomedicine* 2019;**14**:2169–87.